Molecular Therapy
Nucleic Acids
Original Article

Intradermal DNA vaccine delivery using vacuum-controlled, needle-free electroporation

Alison Generotti,[1] Ryne Contreras,[1] Brenden Zounes,[1] Eric Schade,[1] Andrea Kemme,[1] Yatish Rane,[2] Xinggang Liu,[1] Dustin Elwood,[1] Katherine Schultheis,[1] Jeremy Marston,[2] Jay McCoy,[1] Kate Broderick,[1] and Paul Fisher[1]

[1]Inovio Pharmaceuticals, Inc., San Diego, CA 92121, USA; [2]Texas Tech University, Department of Chemical Engineering, Lubbock, TX 79409, USA

Intradermal delivery of DNA vaccines via electroporation (ID-EP) has shown clinical promise, but the use of needle electrodes is typically required to achieve consistent results. Here, delivery of a DNA vaccine targeting the Middle East Respiratory Syndrome Coronavirus (MERS-CoV) is achieved using noninvasive intradermal vacuum-EP (ID-VEP), which functions by pulling a small volume of skin tissue into a vacuum chamber containing noninvasive electrodes to perform EP at the injection site. Gene expression and immunogenicity correlated with EP parameters and vacuum chamber geometry in guinea pigs. ID-VEP generated potent humoral and cellular immune responses across multiple studies, while vacuum (without EP) greatly enhanced localized transfection but did not improve immunogenicity. Because EP was performed noninvasively, the only treatment site reaction observed was transient redness, and ID-VEP immune responses were comparable to a clinical needle-based ID-EP device. The ID-VEP delivery procedure is straightforward and highly repeatable, without any dependence on operator technique. This work demonstrates a novel, reliable, and needle-free delivery method for DNA vaccines.

INTRODUCTION

Plasmid DNA delivery via electroporation (EP) is a clinically proven vaccination platform with potential safety, immunogenicity, and cost advantages compared with traditional vectors. EP is the temporary permeabilization of cell membranes due to electric fields, which greatly enhances DNA uptake within the electroporated tissue. The design of the EP delivery system can directly impact the magnitude and kinetics of immune responses. In the clinic, EP devices typically use needle electrodes inserted into skin or muscle tissue at the site of DNA injection, and due to the reliability of this method, needle-based EP has become the gold standard for in vivo DNA delivery. As an alternative to intramuscular EP (IM-EP), the skin is an attractive target for EP not only due to its accessibility, which permits shallower EP fields, smaller needles, and increased tolerability, but also due to its rich population of immune cells, which may permit fractional dosing.[1–3] Intradermal EP (ID-EP) using a minimally invasive needle array is more tolerable than IM-EP,[4,5] and is also capable of generating potent immune re-sponses at a fraction of the IM dose.[6] The CELLECTRA 3P ID-EP de-livery system has been used in numerous clinical trials to deliver DNA vaccines against Middle East Respiratory Syndrome Coronavirus (MERS-CoV),[7] Ebola virus,[6] and most recently, SARS-CoV-2.[8]

Although needle electrodes are most commonly used in the clinic because they generate reliable electric fields throughout a predetermined tissue depth, the advent of ID-EP has brought new focus to minimally or noninvasive alternatives.[9–11] Noninvasive EP devices usually function by contacting the skin surface with non-penetrating electrodes and conducting current through the highly resistive stratum corneum and the underlying viable epidermis, generating a shallow electric field at the site of the ID plasmid injection. The key disadvantage of noninvasive ID-EP is the risk of the electrodes losing electrical contact during the procedure, which can result in tissue damage, incomplete treatment, and electrical arcing. To overcome this issue, most noninvasive arrays require constant downward pressure, clamping mechanisms, and/or adhesives to prevent electrodes from dislodging or moving during EP.[12–14] These requirements can be logistical barriers to adoption or can contribute to inconsistency and/or operator error that may compromise successful vaccine delivery. Furthermore, when the electrodes of noninvasive EP devices are placed flat against the skin, the resulting electric field is quite shallow due to the large voltage drop across highly resistive stratum corneum and the superficial path of current flow, resulting in primarily keratinocytes, Langerhans cells, and other superficial cell types being transfected.[15,16] In contrast, needle-based EP devices also transfect deeper tissue layers with a more diverse cellular population, which can include dendritic cells, adipocytes, fibroblasts, and myocytes.[17–19]

Here, it was hypothesized that a vacuum chamber could serve to isolate a controlled volume of skin tissue and perform noninvasive EP to induce transfection and immunogenicity following intradermal injection of a DNA vaccine. Combined vacuum + energy delivery systems have previously been developed for a variety of applications, including cosmetics applications for targeted destruction of subcutaneous fat,[20,21] facilitation of endoscopic chemotherapy delivery,[22,23] and even organ-targeted uptake of circulating nucleic acids.[24,25] In this research, the compatibility of such a system with skin delivery of nucleic acids was investigated. Compared with other noninvasive EP methods, vacuum-assisted intradermal EP (ID-VEP) delivery is

Received 12 June 2023; accepted 26 October 2023;
https://doi.org/10.1016/j.omtn.2023.102070.

Correspondence: Paul Fisher, Inovio Pharmaceuticals, Inc., San Diego, CA 92121, USA.
E-mail: paul.fisher@inovio.com

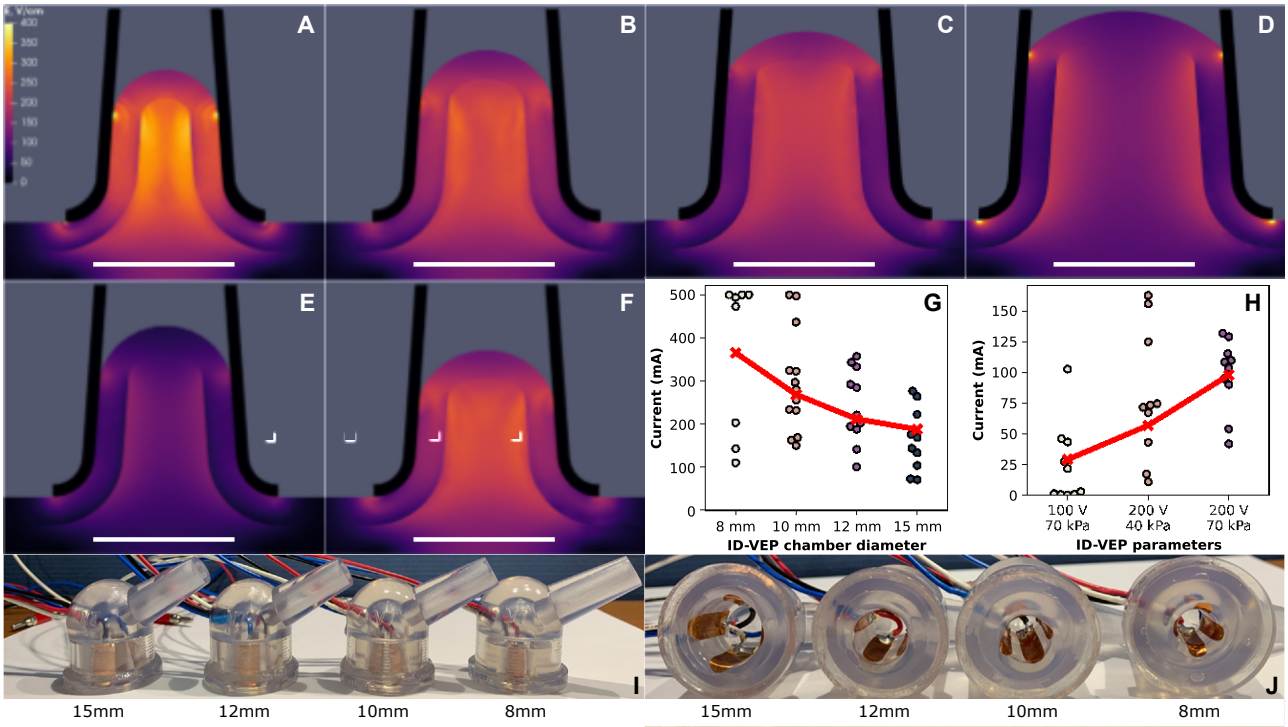

Figure 1. Simulations, electrical readouts, and prototypes

Cross-sectional view of simulated electric field magnitude for various ID-VEP prototypes (A–F), predicted (simulation, red X and dotted line) vs. measured (in vivo, circular data points points) electric current in guinea pigs (G and H), and images of prototype devices used for all in vivo testing (I and J). ID-VEP designs were simulated at 200 V and 70 kPa of vacuum strength for chamber diameters of (A) 8 mm, (B) 10 mm, (C) 12 mm, and (D) 15 mm. ID-VEP of 10-mm chamber diameter was also simulated for pulse intensity/vacuum parameters of (E) 100 V/70 kPa and (F) 200 V/40 kPa. (G) Impact of ID-VEP chamber diameter on electric current for 200 V/70 kPa conditions (data points = in vivo average pulse current, from immunogenicity study 4). (H) Impact of ID-VEP voltage and vacuum strength on electric current for 10 mm ID-VEP diameter (data points = in vivo average pulse current, from immunogenicity study #1). (I) Side and (J) face-on views of ID-VEP prototypes, with the vacuum attachment point highlighted with a yellow asterisk. In (A)–(F), the white scale bar length is 10 mm. Simulation predictions are normalized to the mean electric current of a reference group in each study.

unique because suction can maintain intimate electrode-tissue contact for the duration of the procedure while isolating a large tissue volume, and the deformation of skin allows electric fields to propagate directly through the injection site and multiple tissue layers rather than following a shallow, lateral path along the skin surface. The impact of vacuum pressure, independent of EP, was also studied to see how zones of localized increased pressure within skin tissue impact both transfection and immunogenicity. Computational modeling was used to predict the impact of key ID-VEP design parameters on electric field distribution, and ID-VEP prototypes were built to evaluate in vivo gene expression and immunogenicity in guinea pigs. Immune studies were performed in guinea pigs using a DNA vaccine targeting MERS-CoV as a model system to demonstrate feasibility of this novel, needle-free electroporation system.

RESULTS

Finite volume analysis and prototype development

ID-VEP prototype devices measuring 8 mm, 10 mm, 12 mm, and 15 mm in chamber diameter were rapid prototyped. The same outer housing was used for all prototypes, and a customizable insert was used to control the inner diameter of the ID-VEP chamber. These ID-VEP prototypes were used for all animal studies, and electrodes were cleaned with alcohol wipes after each use.

Figures 1A–1F show a cross-sectional view of the electric field distribution between active electrodes, predicted using finite volume analysis (FVA), for each ID-VEP design and parameter set that was prototyped and tested in vivo. Visually, ID-VEP generates relatively uniform electric fields to all tissue contained inside the EP chamber, with slightly higher field strengths observed within subcutaneous adipose tissue as well as small "hot spots" where skin tissue loses contact with the electrodes. There was a clear inverse association between electric field intensity and ID-VEP chamber diameter for simulations run at 200 V and 70 kPa vacuum strength (Figures 1A–1D). For the 10-mm diameter, decreasing voltage to 100 V appeared to dramatically decrease the electric field strength, while decreasing the vacuum strength to 40 kPa did not visually alter electric field strength but did result in a smaller volume of tissue contained within the EP chamber (Figures 1E and 1F).

To evaluate the accuracy of FVA simulations, the predicted electrical output of each ID-VEP configuration was compared with the in vivo electrical data collected during ID-VEP DNA vaccinations in guinea

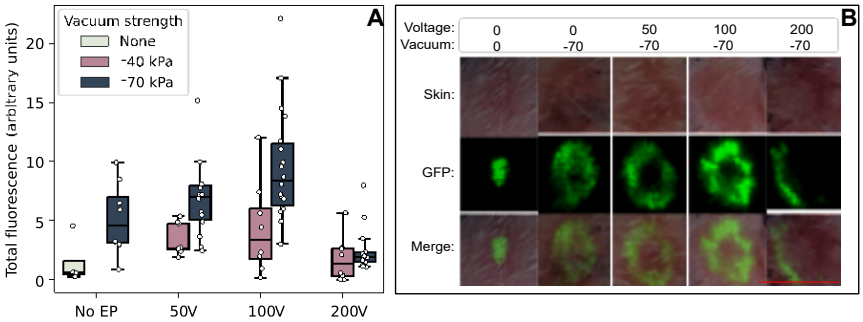

Figure 2. ID-VEP gene expression

(A) Skin fluorescence signal 3 days following VEP delivery of plasmid encoding GFP at various vacuum strengths and voltages in guinea pigs. (B) Representative photographs of treatment sites with GFP expression overlaid 3 days following pGFP delivery for animals receiving ID-VEP delivery at 70 kPa vacuum strength for various voltages. Red scale bar is 10 mm in length. Boxes represent the median and IQR, and whickers extend to the nearest data point up to 1.5*IQR from the nearest hinge

pigs (Figures 1G and 1H). Initial FVA predictions were found to overestimate electric currents (Figure S1). To correct for this overestimation, FVA predictions were normalized to the mean in vivo value of the group with the highest current for each study. After normalization, the FVA predictions accurately predicted the impact of ID-VEP chamber diameter, pulse voltage, and vacuum strength on delivered current. Larger ID-VEP chamber diameter resulted in progressively lower measured and predicted electric current for a pulse voltage of 200 V, spanning a 50% reduction in current as ID-VEP diameter was increased from 8 mm to 15 mm. Additionally, the 10-mm ID-VEP prototype exhibited an approximately 50% reduction in current when vacuum strength was reduced from 70 kPa to 40 kPa for a pulse voltage of 200 V, while current was reduced by 75% when pulse voltage was reduced to 100 V and vacuum strength was maintained at 70 kPa. Notably, the 100-V condition did not consistently deliver pulses; several treatments had a mean current close to 0A.

Gene expression

Studies evaluating in vivo GFP expression of ID-VEP in guinea pigs indicated that stronger vacuum pressure enhances gene expression regardless of EP voltage, and a combination of 100 V ID-VEP voltage and 70 kPa vacuum strength produced the strongest overall GFP expression on the skin surface (Figure 2A). Across injection sites receiving electroporation, increasing vacuum pressure from 40 kPa to 70 kPa doubled GFP expression. Additionally, increasing EP voltage from 50 V to 100 V resulted in a 1.4-fold increase in expression, while further increasing from 100 V to 200 V reduced visible expression by nearly 70%. A detailed summary of statistical test results for ID-VEP GFP expression is available in Table S1. In the absence of electroporation, briefly applying 70 kPa vacuum pressure to the injection site resulted in more than 3-fold higher GFP expression on the skin surface than intradermal injection alone (Welch t test: Fluorescence ratio (95% CI) = 3.39 (1.16–5.62), p = 0.038).

In addition to quantification of GFP fluorescence, expression patterns at treatment sites receiving high vacuum strength were photographed and visually compared (Figure 2B). ID injection of pGFP caused mild erythema even in the absence of vacuum or EP, and resulting GFP expression was concentrated into a small, centralized region. The addition of 70 kPa vacuum strength alone created a broader, circular region of both erythema and transfection, and the further addition of ID-VEP voltages up to 100 V increased the intensity, but not the breadth, of fluorescent signal. At 200 V, the regions with the darkest erythema corresponded with a complete absence of fluorescence signal. Gene expression was also detectable in underlying skin layers following ID-VEP in some samples but was not detectable in the absence of EP, even when vacuum was applied to the injection site (Figure S2).

Immunogenicity

First, the immunological impact of ID-VEP vacuum strength and voltage was quantified using humoral and cellular readouts in guinea pigs vaccinated against MERS-CoV using ID-VEP delivery (Figure 3). All animals (15 of 15) seroconverted after the second vaccination, while after a single vaccination the seroconversion rates were four of five for 70 kPa/200 V, two of five for 40 kPa/200 V, and three of five for 70 kPa/100 V (Figure 3A). At week 4, when peak immuno-genicity was observed, higher EP voltage was significantly associated with stronger binding titers, but higher vacuum strength was not. At week 6—4 weeks after the second vaccination—titers had begun to decrease substantially in animals receiving 100-V delivery, while they remained steady or only slightly decreased in animals receiving 200 V at either vacuum strength. The impact of voltage and vacuum strength on cellular responses was measured via enzyme-linked immunosorbent spot (ELISpot) performed at week 4 of the study (Figure 3B), which indicated that 200-V delivery increased mean cellular responses by approximately 10-fold compared with 100 V, although this effect was not significant. Similar to humoral responses, there was no impact from vacuum strength on cellular response.

In a head-to-head immunogenicity study between ID-EP using intradermal needle electrodes and needle-free ID-VEP, ID-VEP appeared to generate a more rapid humoral response than ID-EP (Figure 4A). By 2 weeks following the first vaccination, all animals in both groups had seroconverted and ID-VEP was associated with significantly higher titers than ID-EP. At subsequent time points following additional vaccinations, there was no significant difference between ID-VEP and ID-EP. Cellular responses, measured at week 2 and week 4 of the study (Figure 4B), increased substantially after the second vaccination for each delivery method, and spot counts were comparable for ID-EP and ID-VEP at each time point.

In a separate study designed to evaluate the impact of vacuum pressure alone (ID-Vacuum) on immunogenicity, ID-VEP was associated with faster and stronger humoral immune responses compared with

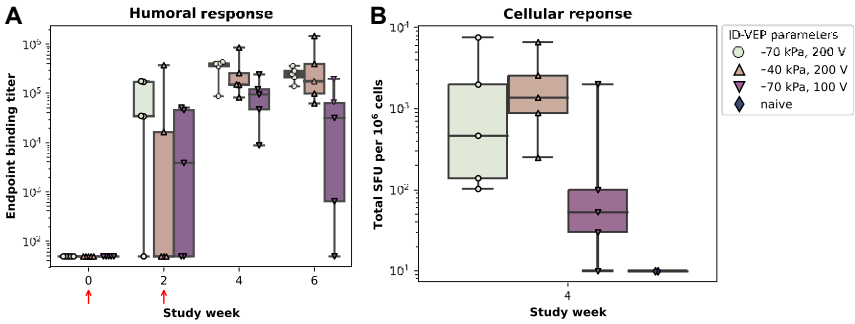

Figure 3. Impact of voltage and vacuum strength on ID-VEP immunogenicity in guinea pigs

Two 50-mg vaccinations were performed at study weeks 0 and 2. (A) Humoral response kinetics of different ID-VEP parameter combinations. Red arrows indicate treatments. (B) Cellular response measured at week 4 following initial vaccination. IFN-g spot-forming units (SFUs) are presented as the sum of five peptide pools' individual responses. All boxplots use the following error bars: boxes represent the median and IQR, and whisker length is the range of all data.

ID-Vacuum or ID delivery alone (Figure 5A). After one vaccination, all ID-VEP animals (five of five) had seroconverted, compared with one of five for ID-Vacuum and zero of five for ID delivery without vacuum or EP. By week 4—2 weeks after a second vaccination—each of the ID-Vacuum and ID groups showed seroconversion in three of five animals. The presence of electroporation was significantly associated with higher titers at week 2, although this effect was not significant at week 4 due to the highly variable, partial responses in the ID and ID-Vacuum groups. In contrast, the use of vacuum alone did not generate any measurable difference in titers compared with ID delivery alone at either time point, although it is notable that the two overall strongest responses at week 4 both received ID-Vacuum delivery. Cellular responses were measured at week 4 (Figure 5B), and the use of electroporation was significantly predictive of higher spot counts while the use of vacuum alone was not.

Next, the impact of ID-VEP chamber diameter on immunogenicity was evaluated. ID-VEP chamber diameter was inversely associated with humoral immune responses, with the smallest (8 mm) diameter generally providing the strongest and most rapid responses (Figure 6A). The relationship between ID-VEP diameter and log-transformed binding titers was significant at each time point, and each millimeter of decreasing ID-VEP diameter was associated with a geometric mean titer increase of approximately 0.2 at week 2, 0.1 at week 4, and 0.09 at week 6. Two weeks after the initial vaccination, the response appeared to be plateauing for the 8-mm and 10-mm diameters. Cellular responses, collected by interferon (IFN)-g ELISpot 2 weeks after the second and third vaccinations, were generally the strongest for ID-VEP chamber diameters ranging from 8 mm to 12 mm, and increasing the diameter to 15 mm appeared to be associated with lower, more variable spot counts, although the impact of diameter on spot counts was not significantly predictive (Figure 6B).

A summary of all statistical comparisons for each of the immunogenicity studies is provided in Table 1.

DISCUSSION

The use of negative pressure, applied directly to internal organs following intravenous infusion of plasmid DNA, has previously been demonstrated to increase transfection at the site where suction is applied.[24,25] Although intravenous injection and targeted pressure to internal organs is not a practical means of DNA vaccine delivery, the finding that negative pressure can disrupt cell membranes to facilitate plasmid delivery agrees with the findings of this research. Furthermore, the use of vacuum fixation to facilitate EP has previously been described, primarily for tissue fixation and homogenization of electric fields during electroporation of mucosal tissue to induce small molecule uptake within intraluminal or superficial tumors during endoscopically guided electrochemotherapy.[22] The EndoVe device uses vacuum to reduce a tumor's interstitial pressure and to immobilize tissue for electrochemotherapy, and this technology was recently shown to be safe and feasible for use in humans.[23,26] However, DNA delivery poses unique challenges compared with small molecule uptake because of its high molecular weight as well as the need to bypass both the plasma membrane and nuclear membrane for successful delivery. Furthermore, the surface of the skin is highly electrically resistive,[27] and it was unknown whether vacuum fixation could provide sufficient coupling at the skin-electrode interface to overcome this barrier. Electrical parameters suitable for small molecule delivery may not be appropriate for delivery of plasmid DNA; while irreversible EP utilizes pulses with an intensity on the order of 1 kV with sub-millisecond pulse durations, reversible EP for DNA delivery typically uses pulse durations multiple orders of magnitude higher (tens or hundreds of milliseconds) with a fraction of the field strength (100 V/cm).[28] Here, ID-VEP was shown to be highly immunogenic, and the magnitude of gene expression and immune responses was directly influenced by the device geometry, the EP pulse parameters, and the vacuum pressure. An ID-VEP chamber diameter of 8 to 10 mm appears optimal, and only a few additional of millimeters of size dramatically reduced immune responses.

Recently, a method of suction-mediated transfection to skin tissue was shown to increase localized transfection and immunogenicity of DNA vaccines in rats.[29] Interestingly, while our results agree with the findings that localized transfection is enhanced through negative pressure alone, we could not reproduce the finding that negative pressure alone also increases immunogenicity of DNA vaccines. Rather, we show in guinea pigs that there was no enhancement in immunogenicity through suction alone, and only the addition of EP led to a dramatic improvement in humoral and cellular immune responses. This may be due to the choice of species for these two different studies; rats have substantially thinner stratum corneum, viable epidermis, and dermis thickness than human skin,[30] whereas guinea pigs have skin

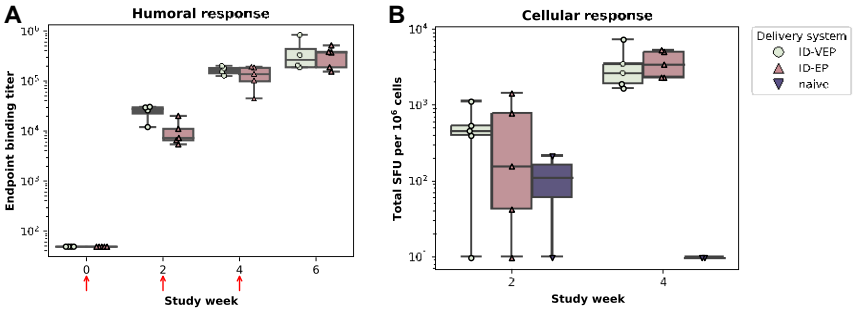

Figure 4. Comparative immunogenicity of pMERS DNA vaccine delivered using ID-EP or ID-VEP in guinea pigs

A total of three 50-mg vaccinations were performed, one every 2 weeks beginning at week 0. (A) Humoral response kinetics of ID-EP and ID-VEP delivery methods. Red arrows indicate treatments. (B) Cellular responses, measured at week 2 and week 4 following initial vaccination. IFN-g spot-forming units (SFUs) are presented as the sum of five peptide pools' individual responses. All boxplots use the following error bars: boxes represent the median and IQR, and whisker length is the range of all data.

more structurally similar to humans, with similarly thick epidermal and dermal layers.[31] These divergent findings highlight the importance of multiple animal models to understand the complex phenomena involved in vacuum-mediated DNA delivery, and also suggest that the addition of electroporation may be necessary when delivering DNA vaccines to thicker, more human-like skin.

Human skin thickness (epidermis + dermis) ranges from 0.5 mm to 2 mm,[32,33] which explains the design of existing ID-EP systems that target the first few millimeters of skin tissue. However, several studies have shown that subdermal cells can be transfected during ID-EP, and prior work from this group showed that subcutaneous fat contributes strongly to DNA vaccine immunogenicity even in the absence of epidermal or dermal transfection.[34] For these reasons, ID-VEP is a rational next step in EP device design, because it can easily immobilize a controlled volume of skin and subcutaneous fat and perform electroporation across that entire volume noninvasively.

FVA and prototype development

FVA was used to prospectively screen the performance of ID-VEP prototype devices and can serve to both inform future design decisions and explain experimental readouts. Reducing pulse voltage from 200 V to 100 V resulted in electric field magnitudes that were generally less than 100 V/cm, which is below the threshold typically associated with successful transfection, although modeling noninvasive electroporation of skin has been historically difficult due to the poorly understood contributions of the stratum corneum.[35] Despite the complex geometry and simplifying assumptions used to build these models, it is promising that the electrical impact of various delivery parameters predicted by FVA closely matches the electrical trends observed in vivo, and these results suggest that FVA may have predictive value when evaluating ID-VEP designs. Furthermore, immune responses (discussed later) also correlated with the observations from simulated electric fields: stronger responses were associated with more intense electric fields.

The FVA performed here assumed that each tissue layer is homogeneous, with electrical conductivity that increases in a sigmoid fashion with electric field strength. Additionally, the stratum corneum was excluded from the model because very thin features can introduce artifacts in finite volume models, and skin was assumed to be a single layer rather than a multilayered composite material. Last, thermal effects were not considered in this model. Because these models consistently overestimated total electric current compared with in vivo, it is possible that further optimization of the conductivity transformation and inclusion of the stratum corneum may yield more accurate results. Once normalized to the baseline in vivo readouts, the models were quite accurate and provide evidence that electric field distributions predicted by these simulations can model ID-VEP device performance.

Gene expression

Gene expression analysis revealed potential synergy between vacuum and EP effects on local protein production. Even in the absence of EP, application of vacuum pressure transfected a large region of superficial skin cells. This change in expression breadth suggests that the skin deformation caused is physically disrupting cell membranes and transfecting cells, and possibly redistributing plasmid laterally through the skin to physically contact more cells. The addition of

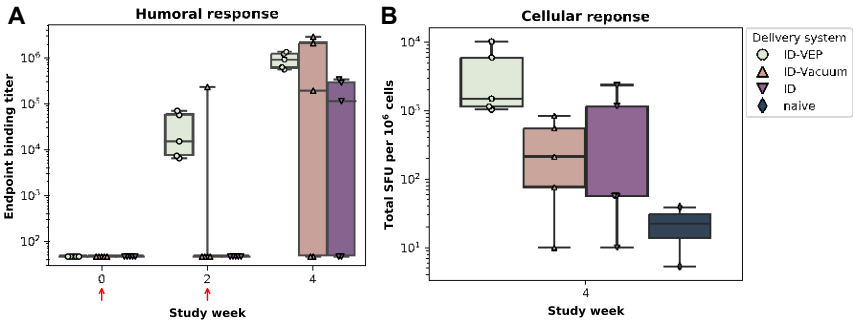

Figure 5. Immunogenicity of pMERS vaccine delivered using either ID-VEP, ID injection followed by vacuum only, or ID injection only in guinea pigs

Two 50-mg vaccinations were performed at study weeks 0 and 2. (A) Humoral responses. Red arrows indicate treatments. (B) Cellular responses, measured at week 4. IFN-g spot-forming units (SFUs) are presented as the sum of five peptide pools' individual responses. All boxplots use the following error bars: boxes represent the median and IQR, and whisker length is the range of all data.

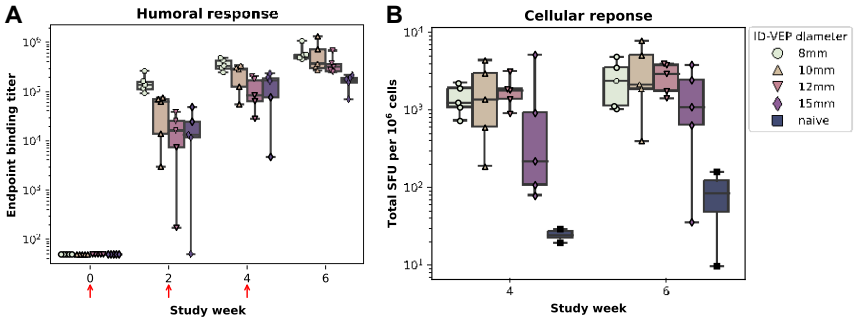

Figure 6. Immunogenicity of pMERS DNA vaccine in guinea pigs, delivered using ID-VEP with chamber diameter ranging from 8 mm to 15 mm

A total of three vaccinations were performed, beginning at week 0. (A) Humoral responses, measured every 2 weeks for 6 weeks. Red arrows indicate ID-VEP treatments. (B) Cellular responses, measured at week 4 and week 6 following initial vaccination. Spot-forming units (SFUs) are presented as the sum of five peptide pools' individual responses. All boxplots use the following error bars: boxes represent the median and IQR, and whisker length is the range of all data.

EP showed a voltage-dependent increase in GFP fluorescence intensity, but not breadth, suggesting that the two techniques may be complementary: vacuum can increase the area of transfection, while EP delivers more plasmid copies over the same area. While superficial expression is primarily due to epidermal skin cells, imaging the underside of skin sections highlights expression in the deeper dermal layers, the subcutaneous adipose tissue, and the panniculus carnosus, which is present in rodent skin. Although expression in the underlying layers was not detectable in all samples, it is notable that expression in deeper tissue layers was only detectable at treatment sites that had received electroporation. This finding suggests that noninvasive ID-VEP is capable of transfecting superficial as well as deeper layers within skin tissue—similar to ID-EP devices that use needle electrodes[17]—whereas intradermal injection alone, with or without

Table 1. Linear regression models used for statistical analysis of each immunogenicity study

Study	Dependent variable	Week	Independent variable	Coefficient	95% CI	p value
1	$\log_{10}$(titer)	2	Voltage (100 vs. 200 V)	0.97	(1.23 to 3.18)	0.356
			Vacuum strength (40 vs. 70 kPa)	1.28	(0.93 to 3.48)	0.231
		4	Voltage (100 vs. 200 V)	0.64	(0.07 to 1.22)	0.031
			Vacuum strength (40 vs. 70 kPa)	0.14	(0.43 to 0.72)	0.603
		6	Voltage (100 vs. 200 V)	1.55	(0.29 to 2.81)	0.020
			Vacuum strength (40 vs. 70 kPa)	0.04	(1.22 to 1.30)	0.951
	$\log_{10}$(SFU)	4	Voltage (100 vs. 200 V)	0.90	(0.12 to 1.92)	0.079
			Vacuum strength (40 vs. 70 kPa)	0.34	(1.36 to 0.68)	0.480
2	$\log_{10}$(titer)	2	Device (ID-EP vs. ID-VEP)	0.41	(0.07 to 0.75)	0.023
		4	Device (ID-EP vs. ID-VEP)	0.14	(0.19 to 0.48)	0.345
		6	Device (ID-EP vs. ID-VEP)	0.02	(0.40 to 0.43)	0.927
	$\log_{10}$(SFU)	2	Device (ID-EP vs. ID-VEP)	0.23	(1.01 to 1.47)	0.676
		4	Device (ID-EP vs. ID-VEP)	0.07	(0.39 to 0.25)	0.608
3	$\log_{10}$(titer)	2	EP (0 vs. 200 V)	1.88	(0.51 to 2.67)	0.011
			Vacuum (0 vs. 70 kPa)	0.74	(0.63 to 2.10)	0.371
		4	EP (0 vs. 200 V)	1.65	(0.86 to 4.16)	0.178
			Vacuum (0 vs. 70 kPa)	0.40	(2.68 to 3.49)	0.798
	$\log_{10}$(SFU)	4	EP (0 vs. 200 V)	1.23	(0.17 to 2.30)	0.027
			Vacuum (0 vs. 70 kPa)	0.01	(1.08 to 1.05)	0.980
4	$\log_{10}$(titer)	2	ID-VEP diameter (mm)	0.19	(0.34 to 0.04)	0.014
		4	ID-VEP diameter (mm)	0.10	(0.17 to 0.02)	0.015
		6	ID-VEP diameter (mm)	0.086	(0.12 to 0.05)	<0.001
	$\log_{10}$(SFU)	4	ID-VEP diameter (mm)	0.069	(0.16 to 0.02)	0.12
		6	ID-VEP diameter (mm)	0.064	(0.15 to 0.03)	0.154

At each week of each study, a linear regression model was fitted to ELISA and ELISpot readouts, and in cases where multiple independent variables are listed, multiple linear regression was performed. Significant results ($p < 0.05$) are bolded.

EP, electroporation; ID-EP, intradermal delivery of DNA vaccines via electroporation; ID-VEP, intradermal vacuum-electroporation; SFU, spot-forming unit.

vacuum, is limited mainly to the superficial epidermis. Future ID-VEP studies should investigate these differences in protein expression patterns at the histological level in order to more fully understand the spatial distribution of transfection and the cell populations involved.

Interestingly, when voltage was increased from 100 V to 200 V, superficial GFP expression in skin sharply declined. This decrease can be attributed to more prominent erythema associated with skin irritation due to higher pulse energy, which effectively quenches visible GFP signal.[36] Therefore, superficial GFP expression readouts are probably unreliable when higher pulse energies are employed, since redness of the tissue may be masking positive signal. It was encouraging to note that none of the ID-VEP treatment sites exhibited any visible signs of irritation beyond transient erythema at the injection site, even at high voltages. Mild muscle contraction was observed during ID-VEP, suggesting that some current flow does reach the underlying muscle tissue. These promising initial results suggest that ID-VEP is well-tolerated and causes minimal tissue damage, although future studies should be conducted to more thoroughly characterize the tissue-level and cell-level responses to the ID-VEP procedure.

Immunogenicity

ID-EP parameters of 200 V pulse intensity and 70 kPa vacuum strength generated the strongest humoral and cellular responses compared with lower vacuum or voltage settings, which agrees with FVA predictions and contrasts with the gene expression findings as explained above. These results raise the possibility that even higher voltages than 200V may continue to enhance immunogenicity, though it must be considered that increased pulse intensities are also associated with discomfort, thermal damage, and irreversible electroporation. Because ID-VEP is intended to be a highly tolerable procedure causing no lasting tissue damage, 200 V was selected as a rational upper limit for these studies, though higher voltages merit further investigation since ID-VEP even at 200 V caused only transient irritation. In addition to pulse intensity alone, future work should also consider other combinations of pulse widths and inter-pulse delays in order to provide a more complete picture of how each electrical parameter impacts immunogenicity and superficial tissue damage.

In a head-to-head comparison between ID-VEP and needle-based ID-EP, ID-VEP generated equivalent cellular responses and superior humoral response kinetics and magnitude through 6 weeks of observation. This improvement may be attributable to the broader, more homogeneous electric field that is generated in ID-VEP compared with needle ID-EP. The reason for such effective electric field coverage is the vacuum component of ID-VEP, which positions skin tissue so electric fields penetrate through all skin layers along two perpendicular axes. These results suggest that ID-VEP overcomes the historical weaknesses of noninvasive EP devices—namely, shallow and inconsistent electric field generation—which have generally led to lower immunogenicity compared with needle-based ID-EP.

Although ID-Vacuum (without EP) delivery generated substantially higher GFP expression than ID delivery (without vacuum or EP), both methods resulted in comparably poor immunogenicity, with virtually no measurable humoral response after one vaccine and partial seroconversion after a second vaccination. Only the combination of vacuum pressure and electroporation was capable of inducing consistent, high-magnitude cellular and humoral responses. This result suggests that transfection alone may not sufficiently predict immune responses to DNA vaccines. Based on these findings, it is proposed that the combination of transfection breadth (due to vacuum pressure) and transfection efficiency (due to EP) act synergistically to increase overall gene expression, while EP is most critical to driving immunogenicity. Previous studies have shown that EP can be synergistically or additively combined with other delivery methods such as sonoporation,[37–39] particle delivery,[40] and jet injection.[41] In addition to its well-characterized enhancement of gene expression, which was corroborated in this study, EP has also been theorized to act as a physical adjuvant since electrical energy produces localized tissue damage that can prompt the localized recruitment of innate and adaptive immune cell types, including macrophages and T cells.[42] This adjuvant effect may further explain the superiority of ID-VEP compared with ID-Vacuum delivery despite their similar gene expression profiles, and it may also explain why smaller ID-VEP diameters (which had stronger electric fields and more electrical "hot spots") were associated with stronger immune responses.

ID-VEP prototypes were designed and built with the objective of encompassing sufficient skin and subcutaneous tissue to transfect an entire 100-mL injection site, but not gathering so much tissue that excess tissue is electroporated needlessly. Therefore, most studies were performed using a 10-mm-diameter ID-VEP chamber, which is similar to the diameter of a standard 100-mL intradermal fluid bleb.[43] The smallest ID-VEP chamber size tested was 8 mm, and smaller sizes were not tested because the entire injection volume would be unable to fit inside the EP chamber. However, larger or smaller ID-VEP devices may be appropriate for different injection volumes or desired depths of transfection.

The work described here used an MERS-CoV DNA vaccine as a model plasmid to develop the ID-VEP system; this research is now of particular relevance due to the ongoing COVID-19 pandemic caused by another coronavirus, SARS-CoV-2. It is encouraging, therefore, that ID-VEP appears to induce rapid and potent humoral responses, which have shown to correlate with protection from infection, hospitalization, and death,[44] as well as strong cellular responses, which we hypothesize will be critical to provide long-lasting and adaptive protection against current and future mutations.[45,46] A well-rounded immune response, generated with a noninvasive, easy-to-use, and well-tolerated ID-VEP device, is an attractive product profile in these pandemic situations where widespread vaccination is required.

Conclusions

This work demonstrates that DNA vaccines delivered via ID-VEP are highly immunogenic—comparable to needle-based ID-EP—and the delivery procedure itself is noninvasive, repeatable, and requires only a few seconds to perform. Design parameters such as chamber

size, pulse intensity, and vacuum strength were shown to influence DNA vaccine immunogenicity and gene expression, and the use of FVA modeling supports the hypothesis that the breadth and magnitude of the electric field can predict and explain performance of ID-VEP systems. Negative pressure was shown to independently enhance transfection and synergized with EP delivery by immobilizing a fixed volume of skin securely against the electrodes lining the EP chamber. This technique provides a reliable, repeatable platform to perform noninvasive EP, and the impact of negative pressure on skin tissue and its interaction with electroporation merits continued research.

MATERIALS AND METHODS

Device design and FVA

SolidWorks (SolidWorks Corp, Concord, MA, USA) was used to generate 3D models of each ID-VEP design. These 3D models were used to create ID-VEP prototype devices that were used for all in vivo studies. To create a 3D model of skin deformation within the ID-VEP chamber, each ID-VEP prototype was placed against guinea pig skin, various vacuum strengths were applied, and the skin deformation was measured under each condition (Figure S3). These measurements were used to create 3D models of skin tissue for each ID-VEP design, and these tissue models were used to perform FVA to model electric field distribution within skin tissue during EP. FVA was performed in ANSYS Fluent (ANSYS Software, Canonsburg, PA, USA). The mesh for each model was generated using the default ANSYS Fluent meshing algorithm. Figure S4 shows an example of a meshed tissue model with ID-VEP electrodes overlaid, as well as the two unique pulses that were modeled between opposing electrode pairs. More details on the mesh are provided in Table S2.

To solve the model, skin was assigned an electrical conductivity of 0.17 S/m, and subcutaneous fat was assigned an electrical conductivity of 0.05 S/m. These properties were based on a publicly available database that aggregates experimental measurements of various tissue properties,[47] as well as historical in-house readouts. Maxwell's equations were solved and a residual error of 10^7 was reached to achieve convergence. The potential difference between the active electrodes (200 V for most models) was defined as a constant boundary condition. To model electric field-dependent increases in tissue conductivity, conductivities were progressively transformed based on electric field magnitude at each iteration using a sigmoid equation for a maximum increase of 4-fold as electric field magnitude approached 600 V/cm (Figure S5). This technique has been previously described as a way to more accurately model the electric field-dependent changes that occur during electroporation in living tissue compared with models using constant conductivity values.[48]

FVA was performed to investigate the impact of the following parameters on electric field distribution: pulse intensity, ID-VEP chamber diameter, and vacuum strength. First, ID-VEP prototypes with an EP chamber measuring 8, 10, 12, or 15 mm were modeled using a pulse intensity of 200 V between active electrodes. Next, the ID-VEP prototype with a chamber diameter of 10 mm was modeled for three different combinations of pulse intensity and vacuum strength: 200 V/70 kPa, 100 V/70 kPa, and 200 V/40 kPa. Paraview software[49] was used to visualize the electric field distributions of each solved model.

Animals

All in vivo studies were performed using female Hartley guinea pigs 12–16 weeks in age and weighing approximately 600 g. For the duration of all procedures, guinea pigs were maintained under anesthesia by inhaled isoflurane. Treatment sites were shaved immediately prior to each procedure. For terminal studies, euthanasia was performed by intracardiac injection of pentobarbital. All animal studies were performed under a protocol approved by an Institutional Animal Care and Use Committee.

Plasmid DNA delivery and electroporation

Intradermal plasmid delivery for all studies consisted of 100-mL ID injection of plasmid DNA onto the flanks of guinea pigs, using a 0.5-mL insulin syringe equipped with a 29-gauge needle. For ID-EP procedures, the CELLECTRA ID Array—a minimally invasive array containing three 3-mm needle electrodes[17]—was immediately inserted into the injection site and EP was performed, delivering two sets of two pulses with an intensity of 0.2A and a pulse duration of 52 ms. For ID-VEP, the vacuum chamber was placed on top of the injection site, the vacuum pump was powered on, and EP was performed once the pressure reached the set-point, delivering two sets of two pulses with an intensity of 200 V and a pulse duration of 100 ms. After EP, the vacuum pump was turned off to release the tissue from the treatment chamber. The duration of the entire ID-VEP procedure, following intradermal DNA injection, was approximately 5–10 s, which is comparable to the duration of an ID-EP procedure. A GEMINI vacuum pump equipped with analog pressure control knob (VWR, Radnor, PA, USA) was used as a vacuum source for all studies. A custom pulse generator was used to deliver the EP pulses.

ID-VEP gene expression

Gene expression studies were conducted in guinea pigs to evaluate the breadth and magnitude of plasmid transfection following ID-VEP with different vacuum and electrical limits. In guinea pigs, ID-VEP delivery of plasmid encoding green fluorescent protein (pGFP, 3,716 base pairs [bp] and human CMV promoter) at a concentration of 0.5 mg/mL was performed, using voltage limits of 50, 100, 100, or 200 V at both low (40 kPa) and high (70 kPa) vacuum strengths. As a control, pGFP was delivered using injection alone (without vac-uum), as well as via injection followed by 70 kPa vacuum (without EP). Skin was excised for analysis 3 days after plasmid delivery, and fluorescence was quantified using a FluorChem R imaging system (ProteinSimple, San Jose, CA, USA). Table S3 summarizes the experimental conditions and number of replicates. Injection sites were also photographed prior to tissue harvest to visually compare signs of superficial tissue damage.

Immunogenicity studies

Four independent immunogenicity studies were performed in guinea pigs, each comparing ID-VEP with different delivery systems or different ID-VEP parameters. Vaccinations used 100 mL intradermal

Table 2. Immunogenicity study designs

Study	Group	n	Delivery	VEP diameter (mm)	Vacuum (kPa)	Voltage (V)	Vaccine schedule (weeks)
1	1	5	ID-VEP	10	40	100	0, 2
	2	5	ID-VEP	10	70	100	
	3	5	ID-VEP	10	70	200	
2	1	5	ID-VEP	10	70	200	0, 2, 4
	2	5	ID-EP	–	–	200	
3	1	5	ID-VEP	10	70	200	0, 2
	2	5	ID-Vac (no EP)	10	70	–	
	3	5	ID (no EP)	–	–	–	
4	1	5	ID-VEP	8	70	200	0, 2, 4
	2	5	ID-VEP	10	70	200	
	3	5	ID-VEP	12	70	200	
	4	5	ID-VEP	15	70	200	

All treatments were performed in guinea pigs, using 100 mL intradermal injection of plasmid encoding MERS-CoV spike protein followed immediately by electroporation.
EP, electroporation; ID-EP, intradermal delivery of DNA vaccines via electroporation; ID-VEP, intradermal vacuum-electroporation; Vac, vacuum.

injection of 50 mg plasmid encoding MERS-CoV spike protein (7,025 bp and human CMV promoter). ID-EP was performed using the CELLECTRA 3P, a minimally invasive device that uses three needle electrodes, while ID-VEP was performed using VEP prototypes with parameters described in Table 2. Vaccinations were performed at week 0 and week 2 of each study, and an additional vaccination was performed at week 4 for two of the four studies. Study 1 was designed to quantify the impact of both vacuum strength and EP voltage on ID-VEP immunogenicity. ID-EP was compared directly with ID-VEP in study 2, while study 3 evaluated each component of ID-VEP (injection, vacuum, and EP) in an additive manner. Study 4 compared different ID-VEP chamber diameters. All studies shared a common study group using a 10-mm-diameter ID-VEP device at 200 V, in order to verify the inter-study repeatability of the ID-VEP procedure. Serum was collected every 2 weeks to measure humoral response kinetics via ELISA, and whole blood was collected at week 4 for ELISpot analysis.

ELISA

ELISA was performed as described previously.[34] Briefly, 96-well plates (Thermo Fisher) were coated overnight with MERS spike protein antigen (Sino Biological, 40069-V08B) in PBS. Plates were then blocked with 3% bovine serum albumin (BSA) for 2 h at room temperature (RT) and washed. Serum in PBS-t containing 1% BSA (Millipore Sigma) was added for 2 h at RT and then washed, and then horseradish peroxidase-conjugated goat anti-guinea pig immunoglobulin G (Millipore Sigma, A7289) was incubated in wells for 1 h at RT. Tetramethylbenzidine substrate solution (VWR) was used to develop color for 6 min, then methylbenzidine stop reagent solution (VWR) was added to halt the reaction. A Synergy HTX plate reader (BioTek Instruments) was used to measure absorbance at 450 nm.

Endpoint binding titers were defined as the intersection point between a 5-parameter logistic curve for each biological replicate at each time point and a single reference curve fitted to the upper limit of the 99% prediction interval calculated at each dilution for all week 0 samples.

ELISpot

ELISpot was performed as described previously.[34,50,51] At 2, 4, and/or 6 weeks following initial vaccination, 3 mL of peripheral blood was collected. Peripheral blood mononuclear cells (PBMCs) were isolated and plated at a density of 1 10^5 cells per well on X-coated 96-well Millipore IP plates. Plated PBMCs were stimulated with 5 MERS peptide pools (GenScript) and IFN-g production was measured using biotinylated mouse monoclonal anti-guinea pig IFN-g antibody and BCIP/NBT detection reagent substrate. A CTL-Immunospot S6 ELISpot plate reader and its included software was used to count spot-forming units (SFU). Spot counts were normalized to baseline by subtracting SFU of wells that did not receive any peptide.

Statistical analysis

Prior to analysis, gene expression data were converted from raw fluorescence values with arbitrary units into ratios relative to a reference group. All immunogenicity data—binding titers for antibody responses and SFU for cellular responses—were log-transformed prior to analysis. For direct comparison of two study groups, a t test with Welch correction was performed. Otherwise, simple linear regression or multiple linear regression was performed at each time point of each study. Since this work is exploratory in nature and the objective of these studies was to generate new hypotheses for future work, multiplicity corrections that account for Type I error but may increase Type II error were not performed.

DATA AND CODE AVAILABILITY

Non-confidential data may be made available upon request to the corresponding author.

SUPPLEMENTAL INFORMATION

Supplemental information can be found online at https://doi.org/10.1016/j.omtn.2023.102070.

ACKNOWLEDGMENTS

Y.R. was supported by funding via an NSF INTERN award (#1934172) during an internship at Inovio, awarded to Jeremy Marston as part of an NSF CAREER award (#1749382).

AUTHOR CONTRIBUTIONS

J.McCoy, K.B., and P.F. were responsible for conceptualization. A.G., R.C., B.Z., X.L., D.E., and P.F. were responsible for data curation. A.G., R.C., B.Z., Y.R., X.L., D.E., K.S., J.Marston, and P.F. were responsible for formal analysis. J.McCoy, K.B., and P.F. were responsible for acquisition of funding at Inovio. A.G., R.C., B.Z., E.S., and A.K. were responsible for experimental investigation. J.McCoy and P.F. were responsible for methodology and project administration. X.L., D.E., Y.R., and J.Marston provided additional resources. B.Z., Y.R., and P.F. were responsible for software. K.B. and P.F. provided supervision. R.C., B.Z., A.G., and P.F. were responsible for validation. B.Z. and P.F. were responsible for visualization. P.F. wrote the original draft, and all authors contributed to review and editing of the subsequent drafts and final manuscript.

DECLARATION OF INTERESTS

A.G., R.C., B.Z., E.S., A.K., X.L., D.E., K.S., J.McCoy, K.B., and P.F. are current or former employees of Inovio and own stock or stock options in the company. P.F., A.K., E.S., J.McCoy, K.B., and A.G. are listed as inventors on a patent application for the ID-VEP technology.

REFERENCES

1. Combadiere, B., and Liard, C. (2011). Transcutaneous and intradermal vaccination. Hum. Vaccin. 7, 811–827. https://doi.org/10.4161/hv.7.8.16274.

2. Egunsola, O., Clement, F., Taplin, J., Mastikhina, L., Li, J.W., Lorenzetti, D.L., Dowsett, L.E., and Noseworthy, T. (2021). Immunogenicity and Safety of Reduced-Dose Intradermal vs Intramuscular Influenza Vaccines: A Systematic Review and Meta-analysis. JAMA Netw. Open 4, e2035693. https://doi.org/10.1001/jamanetworkopen.2020.35693.

3. Schnyder, J.L., De Pijper, C.A., Garcia Garrido, H.M., Daams, J.G., Goorhuis, A., Stijnis, C., Schaumburg, F., and Grobusch, M.P. (2020). Fractional dose of intradermal compared to intramuscular and subcutaneous vaccination - A systematic review and meta-analysis. Travel Med. Infect. Dis. 37, 101868. https://doi.org/10.1016/j.tmaid.2020.101868.

4. Diehl, M.C., Lee, J.C., Daniels, S.E., Tebas, P., Khan, A.S., Giffear, M., Sardesai, N.Y., and Bagarazzi, M.L. (2013). Tolerability of intramuscular and intradermal delivery by CELLECTRA adaptive constant current electroporation device in healthy volunteers. Hum. Vaccin. Immunother. 9, 2246–2252. https://doi.org/10.4161/hv.24702.

5. Hannaman, D., Dupuy, L.C., Ellefsen, B., and Schmaljohn, C.S. (2016). A Phase 1 clinical trial of a DNA vaccine for Venezuelan equine encephalitis delivered by intramuscular or intradermal electroporation. Vaccine 34, 3607–3612. https://doi.org/10.1016/j.vaccine.2016.04.077.

6. Tebas, P., Kraynyak, K.A., Patel, A., Maslow, J.N., Morrow, M.P., Sylvester, A.J., Knoblock, D., Gillespie, E., Amante, D., Racine, T., et al. (2019). Intradermal SynCon Ebola GP DNA Vaccine Is Temperature Stable and Safely Demonstrates Cellular and Humoral Immunogenicity Advantages in Healthy Volunteers. J. Infect. Dis. 220, 400–410. https://doi.org/10.1093/infdis/jiz132.

7. Modjarrad, K., Roberts, C.C., Mills, K.T., Castellano, A.R., Paolino, K., Muthumani, K., Reuschel, E.L., Robb, M.L., Racine, T., Oh, M.D., et al. (2019). Safety and immunogenicity of an anti-Middle East respiratory syndrome coronavirus DNA vaccine: a phase 1, open-label, single-arm, dose-escalation trial. Lancet Infect. Dis. 19, 1013–1022. https://doi.org/10.1016/S1473-3099(19)30266-X.

8. Tebas, P., Yang, S., Boyer, J.D., Reuschel, E.L., Patel, A., Christensen-Quick, A., Andrade, V.M., Morrow, M.P., Kraynyak, K., Agnes, J., et al. (2021). Safety and immunogenicity of INO-4800 DNA vaccine against SARS-CoV-2: A preliminary report of an open-label, Phase 1 clinical trial. EClinicalMedicine 31, 100689. https://doi.org/10.1016/j.eclinm.2020.100689.

9. Lin, F., Shen, X., Kichaev, G., Mendoza, J.M., Yang, M., Armendi, P., Yan, J., Kobinger, G.P., Bello, A., Khan, A.S., et al. (2012). Optimization of Electroporation-Enhanced Intradermal Delivery of DNA Vaccine Using a Minimally Invasive Surface Device. Hum. Gene Ther. Methods 23, 157–168. https://doi.org/10.1089/hgtb.2011.209.

10. Guo, S., Donate, A., Basu, G., Lundberg, C., Heller, L., and Heller, R. (2011). Electrogene transfer to skin using a noninvasive multielectrode array. J. Control. Release 151, 256–262. https://doi.org/10.1016/j.jconrel.2011.01.014.

11. Broderick, K.E., Kardos, T., McCoy, J.R., Fons, M.P., Kemmerrer, S., and Sardesai, N.Y. (2011). Piezoelectric permeabilization of mammalian dermal tissue for in vivo DNA delivery leads to enhanced protein expression and increased immunogenicity. Hum. Vaccin. 7, 22–28. https://doi.org/10.4161/hv.7.0.14559.

12. Heller, L.C., Jaroszeski, M.J., Coppola, D., McCray, A.N., Hickey, J., and Heller, R. (2007). Optimization of cutaneous electrically mediated plasmid DNA delivery using novel electrode. Gene Ther. 14, 275–280. https://doi.org/10.1038/sj.gt.3302867.

13. Heller, R., Cruz, Y., Heller, L.C., Gilbert, R.A., and Jaroszeski, M.J. (2010). Electrically Mediated Delivery of Plasmid DNA to the Skin, Using a Multielectrode Array. Hum. Gene Ther. 21, 357–362. https://doi.org/10.1089/hum.2009.065.

14. Zhang, L., Nolan, E., Kreitschitz, S., and Rabussay, D.P. (2002). Enhanced delivery of naked DNA to the skin by non-invasive in vivo electroporation. Biochim. Biophys. Acta 1572, 1–9. https://doi.org/10.1016/S0304-4165(02)00270-2.

15. Guo, S., Israel, A.L., Basu, G., Donate, A., and Heller, R. (2013). Topical Gene Electrotransfer to the Epidermis of Hairless Guinea Pig by Non-Invasive Multielectrode Array. PLoS One 8, e73423. https://doi.org/10.1371/journal.pone.0073423.

16. Broderick, K.E., Shen, X., Soderholm, J., Lin, F., McCoy, J., Khan, A.S., Yan, J., Morrow, M.P., Patel, A., Kobinger, G.P., et al. (2011). Prototype development and preclinical immunogenicity analysis of a novel minimally invasive electroporation device. Gene Ther. 18, 258–265. https://doi.org/10.1038/gt.2010.137.

17. Amante, D.H., Smith, T.R.F., Mendoza, J.M., Schultheis, K., McCoy, J.R., Khan, A.S., Sardesai, N.Y., and Broderick, K.E. (2015). Skin Transfection Patterns and Expression Kinetics of Electroporation-Enhanced Plasmid Delivery Using the CELLECTRA-3P, a Portable Next-Generation Dermal Electroporation Device. Hum. Gene Ther. Methods 26, 134–146. https://doi.org/10.1089/hgtb.2015.020.

18. Maruyama, H., Ataka, K., Higuchi, N., Sakamoto, F., Gejyo, F., and Miyazaki, J. (2001). Skin-targeted gene transfer using in vivo electroporation. Gene Ther. 8, 1808–1812. https://doi.org/10.1038/sj.gt.3301604.

19. Roos, A.-K., Eriksson, F., Timmons, J.A., Gerhardt, J., Nyman, U., Gudmundsdotter, L., Bråve, A., Wahren, B., and Pisa, P. (2009). Skin Electroporation: Effects on Transgene Expression, DNA Persistence and Local Tissue Environment. PLoS One 4, e7226. https://doi.org/10.1371/journal.pone.0007226.

20. Mulholland, R.S. (2012). Non-Surgical Body Contouring: Introduction of a New Non-Invasive Device for Long-Term Localized Fat Reduction and Cellulite Improvement Using Controlled, Suction Coupled, Radiofrequency Heating and High Voltage Ultra-Short Electrical Pulses. J. Clin. Exp. Dermatol. 03, 1–9. https://doi.org/10.4172/2155-9554.1000157.

21. Duncan, D.I., Kim, T.H.M., and Temaat, R. (2016). A prospective study analyzing the application of radiofrequency energy and high-voltage, ultrashort pulse duration electrical fields on the quantitative reduction of adipose tissue. J. Cosmet. Laser Ther. 18, 257–267. https://doi.org/10.3109/14764172.2016.1157368.

22. Forde, P.F., Sadadcharam, M., Bourke, M.G., Conway, T.A., Guerin, S.R., de Kruijf, M., O'Sullivan, G.C., Impellizeri, J., Clover, A.J.P., and Soden, D.M. (2016). Preclinical evaluation of an endoscopic electroporation system. Endoscopy 48, 477–483. https://doi.org/10.1055/s-0042-101343.

23. Falk Hansen, H., Bourke, M., Stigaard, T., Clover, J., Buckley, M., O'Riordain, M., Winter, D.C., Hjorth Johannesen, H., Hansen, R.H., Heebøll, H., et al. (2020). Electrochemotherapy for colorectal cancer using endoscopic electroporation: a phase 1 clinical study. Endosc. Int. Open 8, E124–E132. https://doi.org/10.1055/a-1027-6735.

24. Shimizu, K., Kawakami, S., Hayashi, K., Kinoshita, H., Kuwahara, K., Nakao, K., Hashida, M., and Konishi, S. (2012). In vivo Site-Specific Transfection of Naked Plasmid DNA and siRNAs in Mice by Using a Tissue Suction Device. PLoS One 7, e41319. https://doi.org/10.1371/journal.pone.0041319.

25. Shimizu, K., Zhang, G., Kawakami, S., Taniguchi, Y., Hayashi, K., Hashida, M., and Konishi, S. (2014). Liver suction-mediated transfection in mice using a pressure-controlled computer system. Biol. Pharm. Bull. 37, 569–575. https://doi.org/10.1248/bpb.b13-00776.

26. Egeland, C., Baeksgaard, L., Johannesen, H.H., Löfgren, J., Plaschke, C.C., Svendsen, L.B., Gehl, J., and Achiam, M.P. (2018). Endoscopic electrochemotherapy for esophageal cancer: a phase I clinical study. Endosc. Int. Open 6, E727–E734. https://doi.org/10.1055/a-0590-4053.

27. Pliquett, U., and Weaver, J.C. (1999). Passive Electrical Properties of Human Stratum Corneum during Application of Electric Fields. In Electricity and Magnetism in Biology and Medicine, F. Bersani, ed. (Springer US)), pp. 259–262. https://doi.org/10.1007/978-1-4615-4867-6_58.

28. Kranjc, M., and Miklavcic, D. (2017). Electric Field Distribution and Electroporation Threshold. In Handbook of Electroporation, D. Miklavcic, ed. (Springer International Publishing), pp. 1043–1058. https://doi.org/10.1007/978-3-319-32886-7_4.

29. Lallow, E.O., Jhumur, N.C., Ahmed, I., Kudchodkar, S.B., Roberts, C.C., Jeong, M., Melnik, J.M., Park, S.H., Muthumani, K., Shan, J.W., et al. (2021). Novel suction-based in vivo cutaneous DNA transfection platform. Sci. Adv. 7, eabj0611. https://doi.org/10.1126/sciadv.abj0611.

30. Wei, J.C.J., Edwards, G.A., Martin, D.J., Huang, H., Crichton, M.L., and Kendall, M.A.F. (2017). Allometric scaling of skin thickness, elasticity, viscoelasticity to mass for micro-medical device translation: from mice, rats, rabbits, pigs to humans. Sci. Rep. 7, 15885. https://doi.org/10.1038/s41598-017-15830-7.

31. Savoji, H., Godau, B., Hassani, M.S., and Akbari, M. (2018). Skin Tissue Substitutes and Biomaterial Risk Assessment and Testing. Front. Bioeng. Biotechnol. 6, 86. https://doi.org/10.3389/fbioe.2018.00086.

32. Diridollou, S., Black, D., Lagarde, J.M., Gall, Y., Berson, M., Vabre, V., Patat, F., and Vaillant, L. (2000). Sex- and site-dependent variations in the thickness and mechanical properties of human skin in vivo. Int. J. Cosmet. Sci. 22, 421–435. https://doi.org/10.1111/j.1468-2494.2000.00037.x.

33. Laurent, A., Mistretta, F., Bottigioli, D., Dahel, K., Goujon, C., Nicolas, J.-F., Hennino, A., and Laurent, P.E. (2007). Echographic measurement of skin thickness in adults by high frequency ultrasound to assess the appropriate microneedle length for intradermal delivery of vaccines. Vaccine 25, 6423–6430. https://doi.org/10.1016/j.vaccine.2007.05.046.

34. Fisher, P.D., Brambila, C.J., McCoy, J.R., Kiosses, W.B., Mendoza, J.M., Oh, J., Yung, B.S., Schultheis, K., Smith, T.R.F., and Broderick, K.E. (2017). Adipose tissue: a new target for electroporation-enhanced DNA vaccines. Gene Ther. 24, 757–767. https://doi.org/10.1038/gt.2017.96.

35. Forjanic, T., and Miklavcic, D. (2018). Numerical study of gene electrotransfer efficiency based on electroporation volume and electrophoretic movement of plasmid DNA. Biomed. Eng. Online 17, 80. https://doi.org/10.1186/s12938-018-0515-3.

36. Hutnick, N.A., Myles, D.J.F., Ferraro, B., Lucke, C., Lin, F., Yan, J., Broderick, K.E., Khan, A.S., Sardesai, N.Y., and Weiner, D.B. (2012). Intradermal DNA Vaccination Enhanced by Low-Current Electroporation Improves Antigen Expression and Induces Robust Cellular and Humoral Immune Responses. https://home.liebertpub.com/hum.10.1089/hum.2012.055.

37. Yamashita, Y.-I., Shimada, M., Tachibana, K., Harimoto, N., Tsujita, E., Shirabe, K., Miyazaki, J.-I., and Sugimachi, K. (2002). Vivo Gene Transfer into Muscle via Electro-Sonoporation. Hum. Gene Ther. 13, 2079–2084. https://doi.org/10.1089/10430340260395929.

38. Escoffre, J.M., Kaddur, K., Rols, M.P., and Bouakaz, A. (2010). In Vitro Gene Transfer by Electrosonoporation. Ultrasound Med. Biol. 36, 1746–1755. https://doi.org/10.1016/j.ultrasmedbio.2010.06.019.

39. Longsine-Parker, W., Wang, H., Koo, C., Kim, J., Kim, B., Jayaraman, A., and Han, A. (2013). Microfluidic electro-sonoporation: a multi-modal cell poration methodology through simultaneous application of electric field and ultrasonic wave. Lab Chip 13, 2144–2152. https://doi.org/10.1039/C3LC40877A.

40. Zhang, L., Widera, G., and Rabussay, D. (2004). Enhancement of the effectiveness of electroporation-augmented cutaneous DNA vaccination by a particulate adjuvant. Bioelectrochemistry 63, 369–373. https://doi.org/10.1016/j.bioelechem.2003.11.011.

41. Hallengärd, D., Bråve, A., Isaguliants, M., Blomberg, P., Enger, J., Stout, R., King, A., and Wahren, B. (2012). A combination of intradermal jet-injection and electroporation overcomes in vivo dose restriction of DNA vaccines. Genet. Vaccines Ther. 10, 5. https://doi.org/10.1186/1479-0556-10-5.

42. Schultheis, K., Smith, T.R.F., Kiosses, W.B., Kraynyak, K.A., Wong, A., Oh, J., and Broderick, K.E. (2018). Delineating the Cellular Mechanisms Associated with Skin Electroporation. Hum. Gene Ther. Methods 29, 177–188. https://doi.org/10.1089/hgtb.2017.105.

43. Simmons, J.A., Davis, J., Thomas, J., Lopez, J., Le Blanc, A., Allison, H., Slook, H., Lewis, P., Holtz, J., Fisher, P., et al. (2019). Characterization of skin blebs from intradermal jet injection: Ex-vivo studies. J. Control. Release 307, 200–210. https://doi.org/10.1016/j.jconrel.2019.06.032.

44. Gilbert, P.B., Montefiori, D.C., McDermott, A., Fong, Y., Benkeser, D.C., Deng, W., Zhou, H., Houchens, C.R., Martins, K., Jayashankar, L., et al. (2021). Immune Correlates Analysis of the mRNA-1273 COVID-19 Vaccine Efficacy Trial. Preprint at medRxiv. https://doi.org/10.1101/2021.08.09.21261290.

45. Dan, J.M., Mateus, J., Kato, Y., Hastie, K.M., Yu, E.D., Faliti, C.E., Grifoni, A., Ramirez, S.I., Haupt, S., Frazier, A., et al. (2021). Immunological memory to SARS-CoV-2 assessed for up to 8 months after infection. Science 371, eabf4063. https://doi.org/10.1126/science.abf4063.

46. McMahan, K., Yu, J., Mercado, N.B., Loos, C., Tostanoski, L.H., Chandrashekar, A., Liu, J., Peter, L., Atyeo, C., Zhu, A., et al. (2021). Correlates of protection against SARS-CoV-2 in rhesus macaques. Nature 590, 630–634. https://doi.org/10.1038/s41586-020-03041-6.

47. Hasgall, P., Di Gennaro, F., Baumgartner, C., Neufeld, E., Lloyd, B., Gosselin, M., Payne, D., Klingenböck, A., and Kuster, N. (2022). IT'IS Database for Thermal and Electromagnetic Parameters of Biological Tissues, Version 4.1. itis.swiss/database. https://doi.org/10.13099/VIP21000-04-1.

48. Corovic, S., Lackovic, I., Sustaric, P., Sustar, T., Rodic, T., and Miklavcic, D. (2013). Modeling of electric field distribution in tissues during electroporation. Biomed. Eng. Online 12, 16. https://doi.org/10.1186/1475-925X-12-16.

49. Ahrens, J., Geveci, B., and Law, C. (2005). ParaView: An End-User Tool for Large-Data Visualization. In Visualization Handbook (Elsevier), pp. 717–731. https://doi.org/10.1016/B978-012387582-2/50038-1.

50. Schultheis, K., Schaefer, H., Pugh, H.M., Yung, B.S., Oh, J., Nguyen, J., Humeau, L., Broderick, K.E., and Smith, T.R. (2019). Optimized Interferon-gamma ELISpot Assay to Measure T Cell Responses in the Guinea Pig Model After Vaccination. J. Vis. Exp. e58595. https://doi.org/10.3791/58595.

51. Schultheis, K., Schaefer, H., Yung, B.S., Oh, J., Muthumani, K., Humeau, L., Broderick, K.E., and Smith, T.R.F. (2017). Characterization of guinea pig T cell responses elicited after EP-assisted delivery of DNA vaccines to the skin. Vaccine 35, 61–70. https://doi.org/10.1016/j.vaccine.2016.11.052.